Inorganic Chemistry

Article

pubs.acs.org/IC

How Does Nishibayashi's Molybdenum Complex Catalyze Dinitrogen Reduction to Ammonia?

Yong-Hui Tian,† Aaron W. Pierpont, and Enrique R. Batista*

Theoretical Division, Los Alamos National Laboratory (LANL), Los Alamos, New Mexico 87545, United States

Supporting Information

ABSTRACT: Recently, Nishibayashi et al. reported a dimolybdenum–dinitrogen complex that is catalytic for complete reduction of dinitrogen to ammonia. This catalyst is different from the Schrock molybdenum catalyst in two fundamental aspects: it contains two metal centers, and the oxidation state is Mo^0 instead of Mo^{III}. We show that a remarkable feature of the bimetallic complex is the bond-mediated delocalized electronic states, resulting from the two metal centers bridged by a dinitrogen ligand. Using first-principles calculations, we found that this property makes the bimetallic complex the effective catalyst, as opposed to the originally postulated monometallic fragment. A favorable reaction pathway is identified, and the nature of the intermediates is examined. Furthermore, studies of the intermediate states led us to propose possible deactivation processes of the catalyst. The finding that the central bimetallic unit (Mo–N_2–Mo) is relevant for catalytic activity may provide a guideline for the development of more efficient dinitrogen-reducing catalysts.

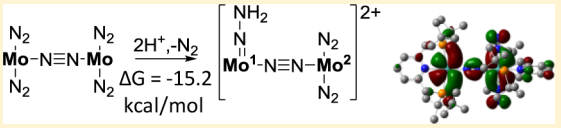

INTRODUCTION

Nitrogen is an essential element for nearly all life forms, but the majority of nitrogen on Earth exists as unreactive dinitrogen (N_2). One of the most important chemical transformations of dinitrogen is the production of ammonia, of which 80% produced globally is used as crop fertilizer. However, because of the inertness of dinitrogen, this transformation consumes 1–2% of the world's energy supply. In organisms, dinitrogen is reduced to ammonia by nitrogenase enzymes at ambient temperatures and pressures. Industrially, nitrogen reduction to ammonia is achieved through the Haber–Bosch process, which requires harsh conditions (150–250 bar and 300–550 °C)[1] and thus is quite energy-intensive. The first reported non-nitrogenase homogeneous catalyst for dinitrogen reduction to ammonia under mild conditions was that of Schrock et al. in 2003 using a molybdenum–dinitrogen complex,[2] $[HIPTN_3N]Mo(N_2)$, where $[HIPTN_3N] = \{3,5\text{-}(2,4,6\text{-}^iPr_3C_6H_2)_2C_6H_3NCH_2CH_2\}_3N\}^{3-}$. A catalytic process has been proposed for the reaction mechanism,[3−5] and the nature of the proposed intermediates was later investigated via both experiments[6−9] and theory.[10−20]

In 2011, Nishibayashi and co-workers reported the second example of a synthetic complex active for catalytic conversion of dinitrogen to ammonia under ambient conditions,[21] where a dinitrogen-bridged dimolybdenum complex **1** (Chart 1) was employed as the catalyst (or the catalyst precursor).[22] The authors found that a yield of 12 equiv of ammonia per Mo atom of the catalyst can be achieved in the presence of a proton source (2,6-lutidinium triflate, [LutH]OTf) and an electron source (cobaltocene, $CoCp_2$), as illustrated in Scheme 1.

Chart 1. Nishibayashi's Molybdenum Complexes (1 and 3) and Originally Postulated Catalyst (2) Formed after Fragmentation

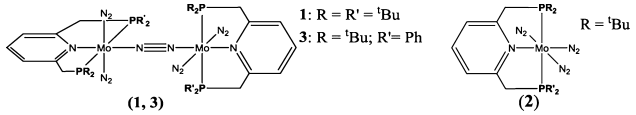

Scheme 1. Catalytic Reduction of Dinitrogen to Ammonia in the Presence of Bimetallic Complex 1

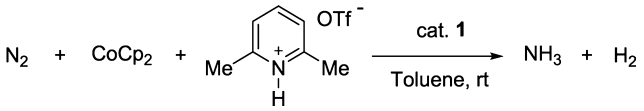

Inspired by the Schrock cycle, a Chatt-like reaction mechanism[23] was postulated, where the bimetallic complex **1** breaks into two monometallic fragments **2** in solution,[21,24] followed by catalytic reduction at a single metal center. However, the proposed intermediates were not observed, and the reaction mechanism remained unclear.

Upon a close comparison of the structures $[HIPTN_3N]Mo(N_2)$ and **1**, it is noted that, in Schrock's catalyst, the metal center is Mo^{III}, whereas in Nishibayashi's complex, the metals are Mo^0. Additionally, five dinitrogen ligands are present in **1**, and hence multiple reactive centers are likely present in a catalytic cycle. In complex **1**, the bridging dinitrogen ligand not only "mechanically" holds the two metal centers in close proximity to form a dimer but also provides an opportunity for electronic communication between the two metal centers. Assuming that the effective Nishibayashi catalyst is a bimetallic complex, the reaction mechanism is expected to show significant differences from Schrock's catalytic cycle. In nature,

Received: January 28, 2014
Published: March 31, 2014

   dx.doi.org/10.1021/ic500221n | Inorg. Chem. 2014, 53, 4177–4183

Scheme 2. Intermediates Involved in Electrochemical Dinitrogen Reduction with the Bimetallic Complex 1[a]

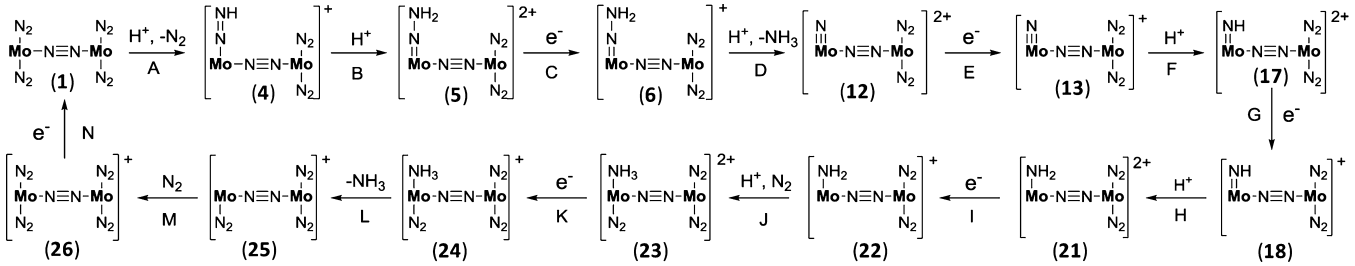

[a]PNP ligands are omitted for clarity.

although it is known that the iron-rich cofactors (including the FeMo cofactor) in nitrogenase enzymes are responsible for dinitrogen reduction,[25,26] there is still debate on the nature of the exact reactive sites.[27,28] Therefore, elucidation of the effective catalysts as a dimer or monomer in Nishibayashi's catalytic systems may shed light on the reaction processes in nitrogenase enzymes.

In addition, elucidation of the reaction pathway and the intermediates of this new catalytic system is essential to understanding the nature of catalytic dinitrogen reduction and finding strategies to design effective catalysts.[22] In this paper, we computationally explore the mechanism of the catalytic reduction of dinitrogen to ammonia in Nishibayashi systems and examine the nature of the catalytic intermediates. It is shown that bimetallic complexes are responsible for the catalytic reduction cycle, instead of the originally postulated monometallic species. The through-bond interactions between the two Mo centers facilitate protonation, making the bimetallic complexes the prime candidates for catalysis. In addition, several possible deactivation processes of the catalyst are examined both kinetically and thermodynamically by comparing the bimetallic complex (**1**) and its phenyl-substituted analogue (**3**). On the basis of the relative hydride stabilities (see the Results and Discussion section) of both analogues, we suggest that the formation of molybdenum hydrides is related to deactivation of the bimetallic catalyst. This conclusion correlates well with the recent experimental observations by Nishibayashi et al. in which the catalytic activity is quenched when the *tert*-butyl groups in complex **1** are substituted by phenyl substituents [structures **1** and **3**, respectively (Chart 1)].[29]

COMPUTATIONAL METHODS

The geometries of all of the compounds in this paper were optimized at the B3LYP level[30] using 6-31G(d,p) basis sets for H, C, N, and P and the Stuttgart effective core potential and corresponding basis set for Mo.[31] The performance of B3LYP has been validated in the literature for dinitrogen reduction catalyzed by molybdenum complexes.[11,12,15,17,18] In addition, the calculated bond lengths of complex **1** agree well with the experimental measurements and are shown in Table S1 in the Supporting Information (SI). The frequencies were calculated at the same level of theory to verify each optimized structure as reactant/product (zero imaginary frequencies) or transition state (one imaginary frequency). Unless stated otherwise, more accurate electronic energies were computed for all optimized structures at the B3LYP level with a relatively larger basis set of 6311+G(2d,2p) for the atoms of H, C, N and P and the same Stuttgart basis set for Mo as before. For $CoCp_2$ and $[CoCp_2]^+$, the multiconfigurational second-order perturbation method (CASPT2),[32] in combination with atomic natural orbital basis sets, was used for calculations of the redox process because of the near-degeneracy of $CoCp_2$.[33] The oxidation energy corresponding to $CoCp_2 \rightarrow [CoCp_2]^+ + e^-$ was calculated as the free-energy difference between the cationic and neutral species. All four d orbitals on molybdenum and eight π orbitals on the cyclopentadienyl (Cp) ligands were included in the active space with 15 or 14 electrons for $CoCp_2$ and $[CoCp_2]^+$, respectively. Free energies were computed at the standard conditions of 1 atm at 298 K. Entropic effects were taken into account using the harmonic approximation for vibrational modes. For consistency with the experiment, solvation in toluene was accounted for (implicitly) using the polarizable continuum model.[34] The transition-state search calculations were carried out using the QST3 method,[35,36] as implemented in the *Gaussian09* package.[37] With the exception of the CASPT2 method, all calculations were performed with the *Gaussian09* package. CASPT2 energies were obtained with the *MOLCAS 7.6* program.[38]

In all of the calculations, the model systems are simplified without considering counteranions, as was done in previous theoretical investigations of the Schrock system.[10−18] In fact, the experiments show that the only an effective lutidimium salt for dinitrogen protonation among the three tested lutidinium salts ([LutH][X]; X =OTf^-, BAr′ [Ar′ = 3,5-$(CF_3)_2C_6H_3$], and Cl^-) is that with X = OTf^-. In the Nishibayashi paper,[21] the pK_a values were assumed to be the same based on the acetonitrile solvent, whereas toluene was used in the actual experiments. We calculated the relative pK_a values (see the SI) of the three types of proton sources, and they show the pK_a order of Cl^- > OTf^- > BAr^-. It is plausible that a proper pK_a value is needed for the effective protonation of the metal center in molybdenum complexes. Too strong an acid like [LutH][BAr] might favor the formation of dihydrogen, whereas too weak an acid like [LutH]Cl may disfavor protonation of the dinitrogen ligands. According to the above statement, we do not expect that the trend would be altered when the counteranions are incorporated in the model systems.

RESULTS AND DISCUSSION

Before discussion of the details of the catalytic processes, Scheme 2 is given to show an overall view of the reaction pathways, which were computationally identified as the most favorable catalytic processes. According to our calculations, the reduction catalyzed by the bimetallic molybdenum complex **1** is thermodynamically more favorable than the catalytic reduction involving the monometallic unit **2**, which is identified in Scheme S1 in the SI. In the following subsections, we will focus on a discussion of the favorable reaction steps, as demonstrated in Scheme 2. A complete energy profile corresponding to the bimetallic processes is provided in Figure S4 in the SI. We also compared the reaction steps for the mono- and bimetallic complexes. The unfavorable bimetallic reaction processes and complete monometallic reaction cycles are reported in the SI.

Unless otherwise stated, **Mo** represents Mo[PNP], where PNP = 2,6-bis(di-*tert*-butylphosphinomethyl)pyridine (see Chart 1 for the structure of PNP). In all of the reported energies, complex **1** is used as the reference state. All of the model systems are composed of the same type and number of

dx.doi.org/10.1021/ic500221n | Inorg. Chem. 2014, 53, 4177−4183

atoms for each reaction step to make the free energies comparable. In the reaction schemes, "H^+" and "e^-" represent proton- and electron-transfer processes, from $[LutH]^+$ and $CoCp_2$, respectively, to the corresponding molybdenum complexes. Accordingly, the protonation and reduction energies are linked to the processes $[LutH]^+ \rightarrow Lut + H^+$ and $CoCp_2 \rightarrow [CoCp_2]^+ + e^-$, respectively. The free-energy changes are denoted by ΔG and electronic energy changes by ΔE. The ground states for all of the chemical species in this paper are calculated to be low-spin states.

The following subsections are organized according to the reaction steps labeled alphabetically in Scheme 2.

Steps A–C ($2H^+/e^-$). As shown in Scheme 3, the initial protonation of the apical dinitrogen ligand of **1** followed by

Scheme 3. Pathways and Relative Free Energies (in kcal mol^{-1}) for $2H^+/e^-$ Addition to Complex 1

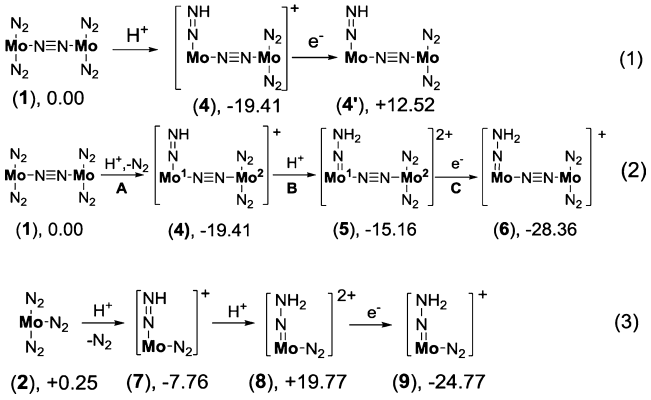

reduction (H^+/e^-) is thermodynamically disfavored.[39] In contrast, the overall process of two successive protonations followed by reduction ($2H^+/e^-$) is exergonic ($\Delta G = -28.36$ kcal mol^{-1}), as shown by eq 2 of Scheme 3. Therefore, successive double protonation is necessary for the first electron addition. One notes that protonation of an apical dinitrogen in **1** is accompanied by a loss of the other apical dinitrogen, leading to complex **4**. One remarkable aspect of the proposed scheme is that the successive double protonation process is also exergonic ($\Delta G = -15.16$ kcal mol^{-1}), which is in contrast to the endergonic protonation for monometallic species **2** (eq 3 in Scheme 3). Given that both the double protonation and subsequent reduction reactions are exergonic, we suggest that either the $2H^+/e^-$ process is part of the catalytic cycle or the hydrazido cationic complex $[NH_2N{=}\mathbf{Mo}(\mu\text{-}N_2)\mathbf{Mo}(N_2)_2]^+$ (**6**) is an important intermediate on the reaction pathway from the bimetallic complex **1** to the actual catalyst. This is consistent with the experimental finding that the hydrazido complex **10** (see Chart 2) can be reduced, leading to the formation of ammonia.[21]

One would expect that the successive double proton addition, giving rise to highly charged species, should be thermodynamically unfavorable, as seen for the monometallic case (eq 3 in Scheme 3). However, for the bimetallic case, the second proton addition becomes considerably less endergonic (**4** → **5**: $\Delta G = 4.25$ kcal mol^{-1}). The reason why the bimetallic structure facilitates successive double protonation is examined below.

Chart 2. Structure of the Hydrazido Complex 10

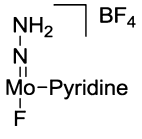

(10)

The conversion from diazenido to hydrazido complexes (**4** → **5** or **7** → **8**) results in increased oxidation states of the metals from Mo^{II} to Mo^{IV}. Therefore, the protonation energies (ΔE^P, defined by eq 4) of the diazenido complexes should be qualitatively correlated to the first ionization potential (IP; see Scheme S5 in the SI for justification for using the first IP). The difference in the protonation energies (represented by $\Delta\Delta E^P$; eq 5) between the dimeric and monomeric systems can be roughly estimated by the difference of the corresponding IP (ΔIP) for $[NH{=}N\mathbf{Mo}(\mu\text{-}N_2)\mathbf{Mo}(N_2)_2]^+$ (**4**) and $[NH{=}N\mathbf{Mo}(N_2)]^+$ (**7**).

$$\Delta E^P \equiv E(\text{hydrazido}) - E(\text{diazenido}) \propto \text{IP} \quad (4)$$

$$\Delta\Delta E = \Delta E^P(\mathbf{4}) - \Delta E^P(\mathbf{7}) \quad (5)$$

$$\Delta\text{IP} = \text{IP}(\mathbf{4}) - \text{IP}(\mathbf{7}) \quad (6)$$

Table 1 lists the calculated protonation energies and the first IP of the diazenido complexes. The protonation energy of dimer **4** is smaller by −0.96 eV than that of the monomer **7**, which is qualitatively consistent with the calculated ΔIP = −1.44 eV. Therefore, we suggest that the favorable double protonation in the bimetallic complexes is attributed to the reduced IP compared to the monometallic complexes.

Table 1. Protonation Energies and IPs of Diazenido Complexes 4 and 7 (Units in eV)

	$\Delta E^{P\,a-c}$	$\Delta\Delta E^{P\,a,b}$	IP	ΔIP
monomer (**7**)	1.07	−0.96	6.54	−1.44
dimer (**4**)	0.11		5.10	

[a]Electronic energies are used. [b]See eqs 3–5 for the definition. [c]The energy changes corresponding to $[LutH]^+ \rightarrow Lut + H^+$ are absorbed into ΔE^P.

The reduced IP in the bimetallic complex **4** is reflected by the change of the atomic charges on the metals upon the second protonation. As shown in Table 2, for both of the monometallic and bimetallic cases, the metal atoms in the hyrazido complexes are more positively charged than those in the diazenido complexes. However, for the bimetallic complexes, the increased charges upon protonation are delocalized on both of the two metal centers, which helps to stabilize the lowest unoccupied molecular orbital (LUMO) state. The delocalized hole can be seen from the lowest

Table 2. Mulliken Charges (Q, in |e|) on the Metal Centers of the Diazenido (4 and 7) and Hydrazido (5 and 8) Complexes[a]

	monomer (**7** → **8**)		dimer (**4** → **5**)	
	7	**8**	**4**	**5**
Q	0.345	0.595	0.379 (0.318)[b]	0.531 (0.414)[b]
ΔQ	0.250		0.152 (0.096)[b]	

[a]The 6-31G(d,p) basis set was used for calculations. [b]The numbers in parentheses correspond to the charges on the nonoxidized Mo center (Mo^2; see Scheme 3 for atom labeling).

dx.doi.org/10.1021/ic500221n | Inorg. Chem. 2014, 53, 4177–4183

unoccupied Kohn–Sham orbital of **5** (Figure 1), where the four d orbitals on the two Mo centers couple through the π orbital

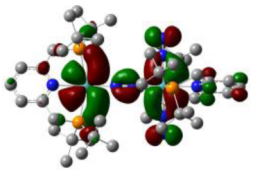

Figure 1. LUMO of structure **5**. Note that four d orbitals from the two Mo centers couple though the bond of the bridging dinitrogen ligand.

of the bridging dinitrogen ligands. Therefore, the reduced IP for the bimetallic complexes is due to the more delocalized holes than those for the monometallic complexes.

In addition to the reactions displayed in Scheme 3, other disfavored protonation/reduction processes of **1** were considered and are shown in Schemes S2 and S3 in the SI, where the second proton addition occurs on another apical dinitrogen ligand coordinated to Mo^1 or Mo^2.

Steps D and E ($3H^+/2e^-$). Reduction of the dimer **6** by $CoCp_2$ is highly endergonic (ΔG = 34.79 kcal mol^{-1}). Proton addition to β-nitrogen leads to the spontaneous loss of an ammonia molecule, giving a molybdenum nitride intermediate (**6** → **12**; eq 7 in Scheme 4), This step is quite exergonic (ΔG

Scheme 4. Computed Pathway for Molybdenum Nitride Formation and NH_3 Release[a]

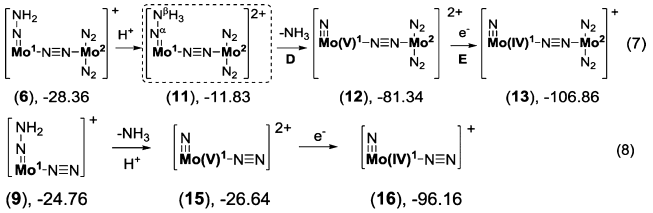

[a]Relative free energies (ΔG) in kcal mol^{-1}.

= −53 kcal mol^{-1}). Subsequent reduction of complex **12** by $CoCp_2$ gives molybdenum(IV) nitride **13**, which is also significantly exergonic (ΔG = −25.52 kcal mol^{-1}).

The potential energy surface in terms of $R_{N^\alpha\cdots N^\beta}$ is examined upon protonation of complex **6**, as presented in Figure 2. The electronic energy changes very little over a wide range, from 1.40 to 1.80 Å. The electronic structure is examined for complex **11** corresponding to $R_{N^\alpha\cdots N^\beta}$ = 1.50 Å along the dissociation path. The characteristic bond lengths and atomic charges of structure **11** are summarized in Table 3. The bond lengths $R_{N^\alpha\cdots N^\beta}$ and R_{Mo-N^α} (Scheme 4) in **11** resemble those of the hydrazido complex **6**. The atomic charges on the two Mo centers do not show significant differences between complexes **6** and **11**, which is in contrast to the much more positively charged metal centers of the molybdenum nitride complex **12**. Moreover, β-nitrogen of structure **11** is more positively charged in comparison to that of the hydrazido complex **6**. The geometry and charge characteristics of **11** are indicative of a protonated hydrazido structure. This indicates that, upon protonation of **6**, the increased positive charges are initially localized on β-nitrogen, giving a long-lived hydrazido species as indicated by the flat region in the potential energy landscape. This is followed by positive charge transfer to the Mo center when the N^α–N^β bond breaks due to thermal energies.

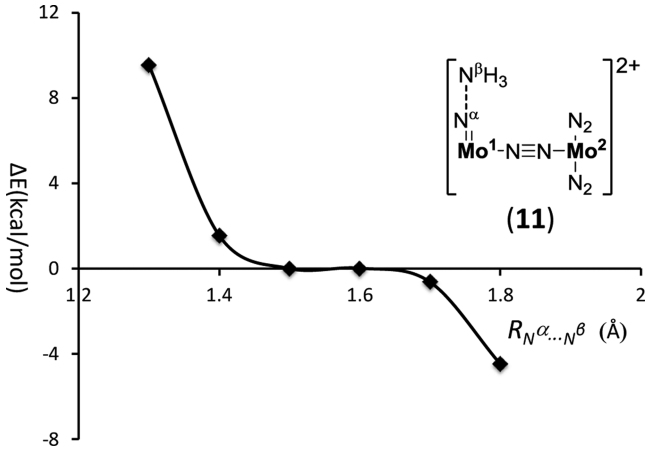

Figure 2. Relaxed potential energy surface scanning along the $R_{N^\alpha\cdots N^\beta}$ distance in structure **11**. $R_{N^\alpha\cdots N^\beta}$ refers to the distance (Å) between the NH_3 and MoN units. ΔE, electronic energy at 0 K. The energies at the separation distance of 1.50 Å are used as a reference.

Table 3. Mulliken Atomic Charges (Q, in |e|) on the Metals and β-Nitrogen and Characteristic Bond Lengths (in Å) in the Intermediates Shown by Equation 7 in Scheme 4[a]

	$Q(Mo^1)$	$Q(Mo^2)$	$Q(\beta\text{-N})$	$R_{N^\alpha\cdots N^\beta}$	R_{Mo-N^α}
6, 1+	0.389	0.314	0.215	1.295	1.919
11, 2+	0.355	0.366	0.618	1.510	1.869
12, 2+	0.527	0.431		break	1.653

[a]See the text for atom labeling.

One notes that, in the nitride complex **12**, both the Mo^1 and Mo^2 centers become more positively charged than those in complex **6**, although protonation takes place only on Mo^1 (as labeled in Scheme 4). The delocalized holes stabilize the cationic molybdenum nitride **12**, which is reflected by the strong exergonicity corresponding to the conversion of **6** → **12**. For comparison, the corresponding protonation and reduction processes of the monometallic hydrazido complex **9** are shown by eq 8 in Scheme 4. Conversion of the hydrazido intermediate to the nitride (**9** → **15**: ΔG = −1.88 kcal mol^{-1}) is greatly disfavored compared to the corresponding conversion (**6** → **12**: ΔG = −52.98 kcal mol^{-1}) for the bimetallic complexes. This justifies the argument that the delocalized holes in the bimetallic complexes stabilize the cationic molybdenum(V) nitride, **12**.

Other protonation/reduction pathways from the bimetallic complex **6** were analyzed (Scheme S6 in the SI) but were thermodynamically disfavored over that shown by eq 7 in Scheme 4.

Steps F and G ($4H^+/3e^-$). Reduction of the molybdenum nitride **13** by $CoCp_2$ is calculated to be highly unfavorable (ΔG = 33.76 kcal mol^{-1}). As shown in Scheme 5, protonation of the nitride complex (**13** → **17**) is calculated to be endergonic (ΔG = 8.78 kcal mol^{-1}). Subsequent reduction is exergonic with an energy change of ΔG = −11.11 kcal mol^{-1}. The overall protonation/reduction (conversion of **13** → **18**) is nearly thermoneutral (ΔG = −2.33 kcal mol^{-1}). In contrast, for monometallic processes as shown by eq 10 in Scheme 5, protonation of the molybdenum nitride (**16** → **19**) is greatly endergonic (ΔG = 39.16 kcal mol^{-1}). Therefore, a bimetallic structure is necessary for protonation of the cationic molybdenum(IV) nitride. Because of strong endergonicity,

dx.doi.org/10.1021/ic500221n | Inorg. Chem. 2014, 53, 4177–4183

Scheme 5. Formation of Molybdenum(III) Imido Intermediates[a]

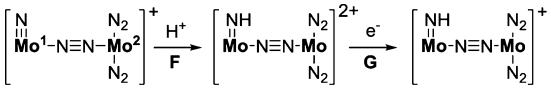

[a]Relative free energies (ΔG) in kcal mol^{-1}.

protonation of monometallic nitrides is not feasible, and thus the monometallic reduction process should stop upon formation of molybdenum nitrides.[40]

As seen from Table 4, upon protonation of the bimetallic nitrides (**13** → **17**), the extra charge is delocalized onto both of

Table 4. Mulliken Atomic Charges (Q, in |e|) of Molybdenum in the Intermediates Shown in Scheme 5

	Monomers		Dimers	
	16	**19**	**13**	**17**
Q	0.356	0.674	0.368 (0.307)[a]	0.567 (0.427)[a]
ΔQ	0.318		0.199 (0.120)	

[a]The numbers in parentheses correspond to the charges in the nonoxidized Mo center.

the two metal centers. This is in contrast to the monometallic process (**16** → **19**), in which the charge increase is localized on a single Mo center. Again, because of the delocalized holes, protonation of bimetallic nitrides is favorable over that of monometallic nitrides.

All other possible protonation and reduction processes are shown in Scheme S7 in the SI, wherein protonation of the apical dinitrogen ligands on the other Mo center is greatly disfavored.

Steps H and I (5H$^+$/4e$^-$). Protonation at the imido ligand of **18** is calculated to be exergonic (ΔG = −5.16 kcal mol^{-1}; Scheme 6), with subsequent reduction being quite favorable

Scheme 6. Protonation/Reduction of the Imido Ligand in Complex 18[a]

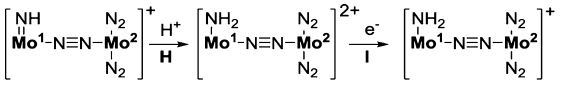

[a]Relative free energies (ΔG) in kcal mol^{-1}.

(ΔG = −21.50 kcal mol^{-1}). As shown in Scheme S8 in the SI, the fifth proton addition to a second apical dinitrogen ligand is significantly disfavored in comparison to protonation of the imido ligand.

Steps J and K (6H$^+$/5e$^-$). Reduction of **22** is endergonic with ΔG = 21.36 kcal mol^{-1}. On the other hand, protonation of the amido ligands is nearly thermoneutral with ΔG = 2.81 kcal mol^{-1} (Scheme 7). Subsequent reduction is again very exergonic (ΔG = −26.76 kcal mol^{-1}). Note that accompanying protonation the complex uptakes another dinitrogen ligand coordinated to the Mo^1 center and trans to the amine ligand. Other pathways were considered (Scheme S9 in the SI), where

Scheme 7. Protonation/Reduction of the Amido Ligand in Complex 22[a]

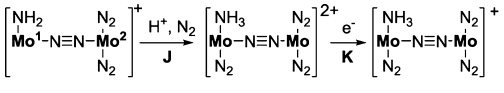

[a]Relative free energies (ΔG) in kcal mol^{-1}.

protonation occurs on the other apical dinitrogen ligands coordinated to Mo^2, but were unfavorable with respect to amido protonation.

Steps L–N (6e$^-$). From the intermediate [NH_3**Mo**(μ-N_2)**Mo**$(N_2)_2$]$^+$ (**24**), the reaction can proceed with the exchange of ammonia with a dinitrogen ligand (Scheme 8). The most

Scheme 8. Sixth Electron Addition and Exchange of Ammonia with Dinitrogen[a]

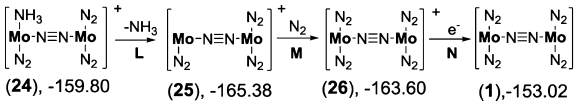

[a]Relative free energies (ΔG) in kcal mol^{-1}.

favorable computed pathway consists of loss of the ammine ligand (**24** → **25**), followed by absorption of a dinitrogen (**25** → **26**) and then reduction (**26** → **1**). The loss of ammonia is slightly exergonic (ΔG = −5.57 kcal mol^{-1}). Subsequent dinitrogen absorption is nearly thermoneutral (ΔG = 1.78 kcal mol^{-1}). Electron addition following ligand exchange is endergonic (ΔG = 10.58 kcal mol^{-1}) and yields the dimolybdenum complex **1**, which completes the catalytic cycle.[41] The other two unfavorable ligand exchange and reduction processes are shown in Scheme S10 in the SI.

FORMATION OF MOLYBDENUM HYDRIDE AND POSSIBLE CATALYST DEACTIVATION PROCESSES

Here we focus on the thermodynamic and kinetic aspects of the formation of molybdenum hydrides because they may be relevant to catalyst deactivation. As shown in Scheme 9, the

Scheme 9. Binding Energy (ΔG in kcal mol^{-1}) of Apical Dinitrogen to Molybdenum

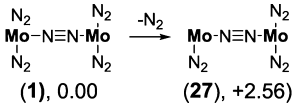

apical dinitrogen ligands are bound loosely to the Mo centers, which enable the direct protonation of molybdenum. The initial protonation of the Mo center (**27** → **29**; Figure 3) along the apical direction is exergonic (ΔE = −28.99 kcal mol^{-1}) and favorable over apical dinitrogen protonation (**27** → **4**: ΔE = −21.14 kcal mol^{-1}). Thus, the thermodynamically favorable formation of molybdenum hydrides prevents protonation of the dinitrogen ligands and might lead to the loss of catalytic activity of molybdenum complexes.

A high-energy barrier [$\Delta E(T)$ = 25.68 kcal mol^{-1}; **27** → **28**] is found for proton transfer from [LutH]$^+$ to molybdenum. Thus, the formation molybdenum hydride **29** is kinetically inhibited by steric hindrance, and hence the reactions can proceed by following the proposed catalytic cycles. On the

dx.doi.org/10.1021/ic500221n | Inorg. Chem. 2014, 53, 4177−4183

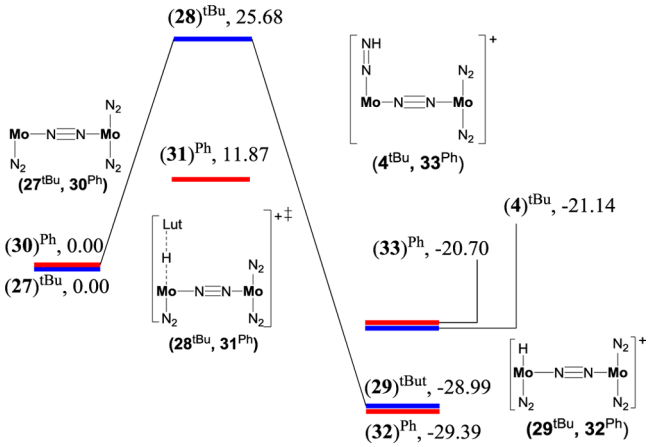

Figure 3. Potential energy diagram for protonation at the Mo centers and at the terminal dinitrogen ligands for both bimetallic complexes, **1** and **3** (or their derivatives **27** and **30**). The superscripts "tBu" and "Ph" are used to distinguish the *tert*-butyl- or phenyl-substituted complexes. The relative electronic energies with thermal correction $[\Delta E(T)]$ are in units of kcal mol^{-1}.

other hand, over a longer time scale, protonation of the metals is likely to occur, deactivating the catalyst.

In a recent paper,[29] Nishibayashi et al. reported a number of bimetallic molybdenum complexes analogous to **1**. When four of the eight *tert*-butyl groups in complex **1** are substituted for phenyl groups, it was found that the phenyl-substituted complex **3** (see Chart 1 for the structure) does not show catalytic activity. On the basis of the similarity of the electronic structures of **1** and **3**, it is reasonable to assume that the proposed reaction cycles are thermodynamically viable for the phenyl-substituted complex **3** as well. Here we focus on the kinetic aspects of the formation of molybdenum hydride. One notes that phenyl groups are less sterically demanding than *tert*-butyl groups. As a consequence, a considerably smaller barrier $[\Delta E(T) = 11.87$ kcal mol$^{-1}]$ was found for proton transfer to molybdenum (**30** → **31**; loss of a dinitrogen ligand from **3** gives structure **30**). This kinetically favorable formation of molybdenum hydride is likely related to the absence of catalytic activity for phenyl-substituted complex **3**.

In complex **1**, the bulky *tert*-butyl groups protect the metals from direct protonation. However, as seen from Scheme 10, a

Scheme 10. Proton-Transfer Process from the Apical Dinitrogen Ligands to Molybdenum[a]

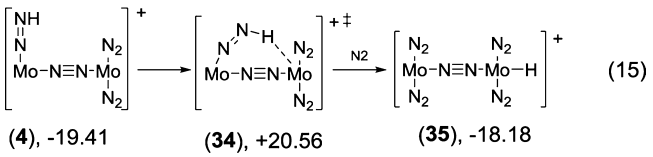

[a]Relative free energies (ΔG) in kcal mol^{-1}.

proton may first protonate the apical dinitrogen ligands and isomerize to complex **35** ($\Delta G = 1.23$ kcal mol^{-1}). In complex **35**, the proton coordinates to the metal in the equatorial plane (see Figure S1 in the SI for the structures). A transition state corresponding to proton transfer was computationally identified with a barrier of $\Delta G = 39.97$ kcal mol^{-1}. Once in the cavity surrounded by the *tert*-butyl groups, the proton in structure **35** may replace the apical dinitrogen ligand by forming the thermodynamically favorable molybdenum hydride complex **29**. Therefore, we suggest that indirect protonation of the metal centers is also responsible for the loss of catalytic activity.

CONCLUSIONS

In Nishibayashi's dinitrogen-reducing system, we found that the bimetallic complex is the effective catalyst instead of the monometallic species that was originally postulated. The dinitrogen-bridged bimetallic structure remained throughout our proposed catalytic cycle, which is consistent with the experimental observation that the dinitrogen bridge is retained upon oxidation of complex **1**.[42] The through-bond interactions of the two metal centers provide an opportunity for charge communication between them, which facilitates the protonation processes and thus makes the bimetallic complexes the prime catalysts. The cationic hydrazido complex is identified as an intermediate in the catalytic processes, which is in agreement with the experimental finding that the hydrazido complex **10** can be reduced with the formation of ammonia. One remarkable feature of the proposed mechanism is that all of the intermediates except complex **1** in the catalytic cycle are cationic species. The intermediates bearing two positive charges appear in our proposed reaction cycle, which is attributed to the bond-mediated dimetal center structure. The finding that charge communication between the two metal centers is relevant for catalytic activity may offer a guideline to the design and synthesis of efficient dinitrogen-reducing catalysts. Our kinetic and thermodynamic study demonstrates that the formation of molybdenum hydrides is relevant to catalyst deactivation. We have shown that protonation of the Mo center is kinetically disfavored for Nishibayashi's system, which helps to explain the robustness of the catalyst. On the other hand, for the phenyl-substituted analogue of complex **1**, direct proton transfer from $[LutH]^+$ to the metal centers is feasible. This is in agreement with the experimental observation that the phenyl-substituted dimolybdenum complex does not show catalytic dinitrogen reduction activity.

ASSOCIATED CONTENT

Supporting Information

Thermodynamically disfavored reaction pathways, catalytic reduction cycles involving the monometallic complex **2**, justification for the correlation between the first IP and protonation energy, selected bond lengths of complex **1** optimized at the theory level described in the text, relative pK_a values for the lutidinium salts, and dissociation energies of the intermediate complexes shown in Scheme 2. This material is available free of charge via the Internet at http://pubs.acs.org.

AUTHOR INFORMATION

Corresponding Author

*E-mail: erb@lanl.gov.

Present Address

[†]College of Life Sciences Sichuan University Chengdu, Sichuan 610064 China. E-mail: yonghuitian@scu.edu.cn.

Notes

The authors declare no competing financial interest.

ACKNOWLEDGMENTS

This research was sponsored by the Laboratory Directed Research and Development program at LANL. LANL is operated by Los Alamos National Security, LLC, for the

National Nuclear Security Administration of the U.S. Department of Energy under Contract DE-AC5206NA25396.

REFERENCES

(1) Smil, V. *Enriching The Earth: Fritz Haber, Carl Bosch, and the Transformation of World Food Production*; MIT Press: Boston, 2004.
(2) Yandulov, D. V.; Schrock, R. R.. *Science* **2003**, *301*, 76−78.
(3) Schrock, R. R. *Angew. Chem., Int. Ed.* **2008**, *47*, 5512−5522.
(4) Weare, W. W.; Dai, X.; Byrnes, M. J.; Chin, J. M.; Schrock, R. R.; Müller, P. *Proc. Natl. Acad. Sci. U.S.A.* **2006**, *103*, 17099−17106.
(5) Schrock, R. R. *Acc. Chem. Res.* **2005**, *38*, 955−962.
(6) Yandulov, D. V.; Schrock, R. R. *J. Am. Chem. Soc.* **2002**, *124*, 6252−6253.
(7) Yandulov, D. V.; Schrock, R. R.; Rheingold, A. L.; Ceccarelli, C.; Davis, W. M. *Inorg. Chem.* **2003**, *42*, 796−813.
(8) Yandulov, D. V.; Schrock, R. R. *Inorg. Chem.* **2005**, *44*, 1103−1117.
(9) Munisamy, T.; Schrock, R. R. *Dalton Trans.* **2012**, *41*, 130−137.
(10) Reiher, M.; Le Guennic, B.; Kirchner, B. *Inorg. Chem.* **2005**, *44*, 9640−9642.
(11) Studt, F.; Tuczek, F. *Angew. Chem., Int. Ed.* **2005**, *44*, 5639−5642.
(12) Le Guennic, B.; Kirchner, B.; Reiher, M. *Chem.—Eur. J.* **2005**, *11*, 7448−7460.
(13) Neese, F. *Angew. Chem., Int. Ed.* **2006**, *45*, 196−199.
(14) Schenk, S.; Le Guennic, B.; Kirchner, B.; Reiher, M. *Inorg. Chem.* **2008**, *47*, 3634−3650.
(15) Magistrato, A.; Robertazzi, A.; Carloni, P. *J. Chem. Theory Comput.* **2007**, *3*, 1708−1720.
(16) Studt, F.; Tuczek, F. *J. Comput. Chem.* **2006**, *27*, 1278−1291.
(17) Schenk, S.; Reiher, M. *Inorg. Chem.* **2009**, *48*, 1638−1648.
(18) Schenk, S.; Kirchner, B.; Reiher, M. *Chem.—Eur. J.* **2009**, *15*, 5073−5082.
(19) Khoroshun, D. V.; Musaev, D. G.; Morokuma, K. *Mol. Phys.* **2002**, *100*, 523−532.
(20) (a) Laplaza, C. E.; Cummins, C. C. *Science* **1995**, *268*, 861−863. (b) Cummins, C. C. *Chem. Commun.* **1998**, 1777−1786.
(21) Arashiba, K.; Mikyake, Y.; Nishibayashi, Y. *Nat. Chem.* **2011**, *3*, 120−125.
(22) Schrock, R. R. *Nat. Chem.* **2011**, *3*, 95−96.
(23) Chatt, J.; Dilworth, J. R.; Richards, R. L. *Chem. Rev.* **1978**, *78*, 589−625.
(24) MacLeod, K. C.; Holland, P. L. *Nat. Chem.* **2013**, *5*, 559−565.
(25) Burgess, B. K.; Lowe, D. J. *Chem. Rev.* **1996**, *96*, 2983−3012.
(26) Schwarz, G.; Mendel, R. R.; Ribbe, M. W. *Nature* **2009**, *460*, 839−847.
(27) Seefeldt, L.; Hoffman, B. M.; Dean, D. R. *Annu. Rev. Biochem.* **2009**, *78*, 701-722.
(28) Anderson, J. S.; Rittle, J. R.; Peters, J. C. *Nature* **2013**, *501*, 84−88.
(29) Kinoshita, E.; Arashiba, K.; Kuriyama, S.; Miyake, Y.; Shimazaki, R.; Nakanishi, H.; Nishibayashi, Y. *Organometallics* **2012**, *31*, 8437−8443.
(30) Becke, A. D. *J. Chem. Phys.* **1993**, *98*, 5648−5652.
(31) Bergner, A.; Dolg, M.; Kuechle, W.; Stoll, H.; Preuss, H. *Mol. Phys.* **1993**, *80*, 1431−1441.
(32) Roos, B. O.; Taylor, P. R.; Siegbahn, P. E. M. *Chem. Phys.* **1980**, *48*, 157−173.
(33) CASPT2 and B3LYP methods gave about a 0.39 eV difference in terms of the oxidation energies corresponding to the process of $Co(Cp)_2 \rightarrow Co(Cp)_2^+ + e$.
(34) Scalmani, G.; Frisch, M. J. *J. Chem. Phys.* **2010**, *132*, 114110.
(35) Peng, C.; Schlegel, H. B. *Isr. J. Chem.* **1993**, *33*, 449−454.
(36) Peng, C.; Ayala, P. Y.; Schlegel, H. B.; Frisch, M. J. *J. Comput. Chem.* **1996**, *17*, 49−56.
(37) Frisch, M. J.; Trucks, G. W.; Schlegel, H. B.; Scuseria, G. E.; Robb, M. A.; Cheeseman, J. R.; Scalmani, G.; Barone, V.; Mennucci, B.; Petersson, G. A.; Nakatsuji, H.; Caricato, M.; Li, X.; Hratchian, H. P.; Izmaylov, A. F.; Bloino, J.; Zheng, G.; Sonnenberg, J. L.; Hada, M.; Ehara, M.; Toyota, K.; Fukuda, R.; Hasegawa, J.; Ishida, M.; Nakajima, T.; Honda, Y.; Kitao, O.; Nakai, H.; Vreven, T.; Montgomery, J. A., Jr.; Peralta, J. E.; Ogliaro, F.; Bearpark, M.; Heyd, J. J.; Brothers, E.; Kudin, K. N.; Staroverov, V. N.; Kobayashi, R.; Normand, J.; Raghavachari, K.; Rendell, A.; Burant, J. C.; Iyengar, S. S.; Tomasi, J.; Cossi, M.; Rega, N.; Millam, N. J.; Klene, M.; Knox, J. E.; Cross, J. B.; Bakken, V.; Adamo, C.; Jaramillo, J.; Gomperts, R.; Stratmann, R. E.; Yazyev, O.; Austin, A. J.; Cammi, R.; Pomelli, C.; Ochterski, J. W.; Martin, R. L.; Morokuma, K.; Zakrzewski, V. G.; Voth, G. A.; Salvador, P.; Dannenberg, J. J.; Dapprich, S.; Daniels, A. D.; Farkas, Ö.; Foresman, J. B.; Ortiz, J. V.; Cioslowski, J.; Fox, D. J. *Gaussian 09*, revision C.01; Gaussian, Inc.: Wallingford, CT, 2009.
(38) *MOLCAS*: a program package for computational chemistry: Karlström, G.; Lindh, R.; Malmqvist, P.-Å.; Roos, B. O.; Ryde, U.; Veryazov, V.; Widmark, P.-O.; Cossi, M.; Schimmelpfennig, B.; Neogrady, P.; Seijo, L. *Comput. Mater. Sci.* **2003**, *287*, 222−239.
(39) Transfer of an electron from $CoCp_2$ to **1** is calculated to be highly endergonic (ΔG = 64.19 kcal mol^{-1}). Therefore, reduction preceding protonation (e^-/H^+) is ruled out.
(40) For the monometallic nitride **16**, the process of reduction preceding protonation (e^-/H^+) is disfavored as well because of the strongly endergonic reduction step, as shown in Scheme S4a in the SI.
(41) Protonation of the apical dinitrogen ligands of complex **26** is highly endergonic (ΔG = 31.98 kcal mol^{-1}).
(42) As shown in Figure S3 in the SI, for all the intermediates shown in Scheme 2, the cleavage processes are endergonic.